Article

Atomic Oxygen-Resistant Epoxy-amines Containing Phenylphosphine Oxide as Low Earth Orbit Stable Polymers

Witold K. Fuchs, Catherine Sarantes, Nathaniel Prine, Xiaodan Gu, Derek L. Patton,
and Jeffrey Wiggins*

Cite This: https://dx.doi.org/10.1021/acsapm.0c01017

Read Online

ACCESS | Metrics & More | Article Recommendations | Supporting Information

ABSTRACT: Atomic oxygen (AO) attacks carbon-fiber reinforcing polymers on the surfaces of spacecraft in low Earth orbit and threatens safe spacecraft operation and service life. Incorporating phenylphosphine oxide (PPO) groups into polymer chains offers a self-regenerating method of protection from AO but remains poorly understood. Herein, epoxies containing PPO groups were synthesized with increasing concentrations of phosphorus [P] from 0 to 8 wt % to investigate their AO resistance. Thin films of PPO-containing epoxies were exposed to AO via oxygen plasma etching and characterized by interferometry, X-ray photoelectron spectroscopy, and atomic force microscopy—infrared spectroscopy. Measurements confirmed that the exposure of these materials to AO produces a passivation phosphate (PO_x) layer on the surface of the sample, resulting in up to 100X decrease in AO erosion rates. Furthermore, key insights into the relationship between initial [P], passivation layer surface topology, and polymer depth profiles were obtained. Crucially, the results indicate that these materials advantageously did not exhibit linear erosion rates when exposed to AO, in contrast to most organic polymers, and their AO resistance can be readily tuned via synthetic incorporation of monomers with varying [P].

KEYWORDS: phenylphosphine oxide, epoxy, atomic oxygen, space composites, thermoset polymers
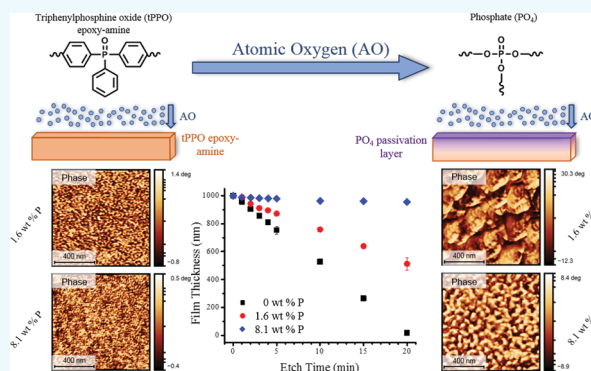
INTRODUCTION

Advanced composite materials are promising candidates in space applications due to their high modulus and strength-to-weight ratios.[1] However, atomic oxygen (AO) attack to polymer materials on the surface of spacecraft in low Earth orbit (LEO) is a serious problem that threatens spacecraft composite service life.[2−4] Several in-orbit tests have been performed by the European Space Agency, Japan Aerospace Exploration Agency, and the National Aeronautics and Space Administration (NASA) to understand the AO resistance of various materials.[5−7] When unprotected polymers undergo AO attack, they suffer from surface erosion, mass loss, and loss of mechanical properties.[8−10]

Typically, polymeric materials are protected from AO by the deposition of coatings such as aluminum oxide, silicon dioxide, tin oxide, or indium tin oxide base.[11] However, not only are there restrictions on the shape and size of polymeric materials that can be protected with coatings but thermal expansion coefficient (CTE) mismatches between the coating and the composite can lead to cracking during thermal cycling.[12] Such cracking neutralizes the protective effect of the coating and exposes the underlying material to AO erosion. Therefore, it is essential to develop new polymeric materials with high AO resistance to prolong the spacecraft lifespan.

A major thrust in current research has focused on the incorporation of AO-resistant moieties such as phosphine oxide or siloxane directly into the backbone of polymers to avoid the shape and CTE limitations of coatings.[11,13,14] In particular, the strategy of incorporating phenylphosphine oxide (PPO) groups into polymers has attracted widespread attention as a particularly effective way of imparting AO resistance.[8,11,15] Connell and co-workers at the NASA Langley Research Center pioneered a series of PPO-containing polymers and demonstrated their AO and oxygen plasma resistance.[16−19] It was demonstrated that polymers containing 3−7 wt % phosphorus exhibited high glass transition temperatures (T_g) and Young's moduli.[11] Based on these developments, a series of polyimides containing PPO have been prepared, but studies to understand the potential of PPO resistance to AO in other polymers have been limited.[8,11]

A

Epoxy matrices are the most commonly used polymers for carbon-fiber reinforcing polymers (CFRPs) in space applications.[14] Degradation of epoxies by AO has been shown to significantly reduce the performance of materials, which is particularly detrimental to deployable structures.[20] A recent work has shown that prolonged AO exposure to epoxy CFRPs can entirely erode the matrix polymer and expose the underlying fiber.[20] Epoxies containing PPO have previously been explored as candidates for flame-retardant materials, with a majority of work focusing on the preparation of PPO diamines; however, their resistance to AO erosion has not been studied.[21−23]

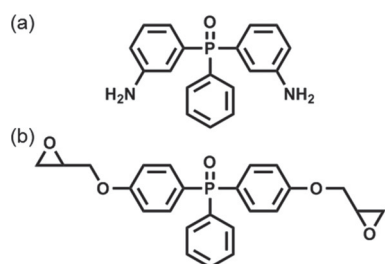In the present work, a bisglycidyl PPO (bGE-tPPO) and a diamine PPO (bA-tPPO) (Figure 1) were prepared. The

Figure 1. Structure of synthesized (a) bA-tPPO and (b) bGE-tPPO monomers.

resultant monomers, along with tetraglycidylmethylene diani-line (TGDDM), diglycidylether bisphenol-A (DGEBA), and 3,3-diaminodiphenylsulfone (3,3-DDS) (Figure 2), were
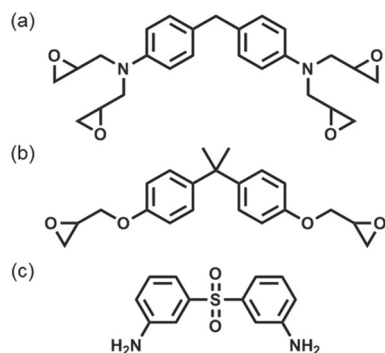

Figure 2. Structure of purchased (a) TGDDM, (b) DGEBA, and (c) 3,3-DDS monomers.

polymerized to prepare epoxy-amines with high (>8 wt % P) phosphorus contents. The effect of systematically varying phosphorus [P] on the AO resistance and the surface morphology of the resultant passivation layer was investigated. The formed passivation layer reduced the bulk degradation of an aerospace epoxy matrix >100X in comparison to the neat polymer. Finally, X-ray photoelectron spectroscopy (XPS) depth profile experiments and atomic force microscopy−infrared spectroscopy (AFM-IR) provided key insights into the efficacy of the formed passivation layer and the depth of AO degradation in the prepared epoxy matrices.

■ **EXPERIMENTAL SECTION**

Materials. Phenylphosphonic dichloride (97%), 4-bromofluoro-benzene (99%), and fuming hydrochloric acid (37%) were purchased from ACROS Organics and used without further purification.

Triphenylphosphine oxide (99%) and anhydrous tin(II) chloride (99%) were purchased from Alfa Aesar and used without further purification. Benzyltrimethylammonium chloride (99%) and epichlor-ohydrin (99%) were purchased from TCI America and used without further purification. Silicon wafers (orientation <100>, p type) were purchased from University Wafer. Ultra high purity grade oxygen gas was purchased from Airgas.

The following materials were used as received: N,N,N',N'-tetraglycidyl-4,4′-diaminodiphenylmethane (TGDDM, MY721, EEW = 113, Huntsman) and 3,3′-diaminodiphenylsulfone (3,3′-DDS. Royce Chemical Corp., >99% pure, 4 μm particle size).

Epoxide Monomer Synthesis. The precursor to bGE-tPPO, bis-4-hydroxyphenylphospine oxide (4,4-BH-tPPO), was synthesized using Grignard chemistry with a fluorinated precursor approach due to its cost-effectiveness and high yield.[24] The fluorinated precursor does pose a potential hazard of generating hydrofluoric acid during the titration step; however, judicious safety measures are sufficient to prevent HF formation.

The synthesis route to bGE-tPPO is shown in Scheme 1. The details are as follows.

Scheme 1. Synthesis of bis-4-Fluorotriphenylphosphine Oxide (4,4-BF-tPPO), bis-4-Hydroxytriphenylphosphine Oxide (4,4-BH-tPPO), and Bis-4-Glycidylethertriphenylphosphine Oxide (bGE-tPPO)
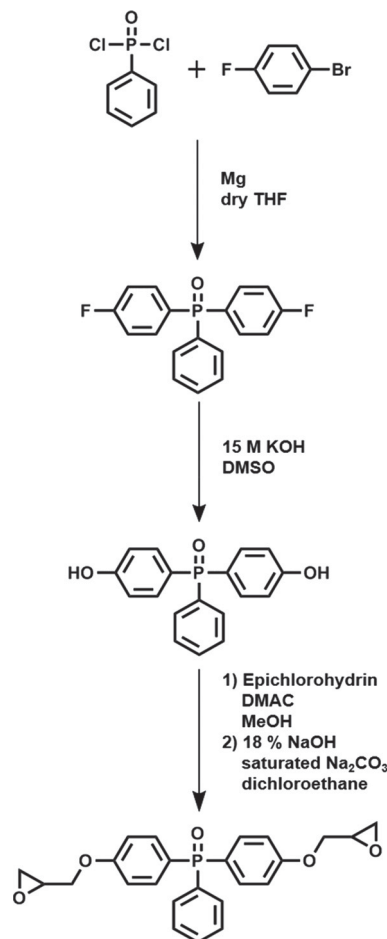
Synthesis of bis-4-Fluorotriphenylphosphine Oxide (4,4-BF-tPPO). To a 1000 mL three-neck round-bottom flask equipped with a mechanical stirrer, addition funnel, condenser, and N_2 inlet/outlet, magnesium turnings (20.91 g, 0.86 mols) were dissolved in dry THF (700 mL) as much as possible overnight. The following day, 4-bromofluorobenzene (150 g, 0.86 mols, 2 eq.) was transferred to an addition funnel and added over 3 h, maintaining the solution at −5

°C. The solution was then stirred for 3 h. To this solution mixture, phenylphosphonic dichloride (83.56 g, 0.43 mols, 1 eq.) was added dropwise through an addition funnel. After addition, the solution was heated to 50 °C and stirred overnight. The following day, 10% aqueous sulfuric acid was added to acidify the mixture and the solution was diluted with deionized water. Diethyl ether was added in order to separate the solution into organic and aqueous phases. The organic layer was collected and the aqueous layer was extracted with diethyl ether. The collected organic phase was dried over MgSO$_4$ and rotary evaporated to afford a viscous liquid. The crude product was recrystallized from a 50/50 solution of hexane and toluene to a yield of 96%. ^{1}H NMR 600 MHz (DMSO-d$_6$): δ 7.4 4H ddd, δ 7.5 2H dddd, δ 7.6–7.75 4H ddd, 2H dtd, 1H tt. ^{31}P NMR 600 MHz (DMSO-d$_6$): δ 24.96 1P s (Figure S1).

Synthesis Of bis-4-Hydroxytriphenylphosphine Oxide (4,4-Bh-tppo). 4,4-BF-tppo (40 g, 0.12 mols, 1 eq.) was charged with distilled DMSO (150 mL) and 15 M KOH (80 mL, 10 eq.) into a 500 mL three-neck round-bottom flask equipped with a mechanical stirrer, refluxing condenser, and N$_2$ inlet/outlet. The reaction mixture was refluxed for 8 h at 130 °C. Over the reaction duration, the color of the mixture gradually changed from white, to clear, to pink, to clear yellow. After the reaction mixture cooled, the mixture was poured into deionized (DI) H$_2$O and titrated to pH 3 using dilute HCl. The resulting white precipitate was filtered through an acid-resistant filter paper and dried overnight. The product was then recrystallized from an 80/20 mixture of MeOH/DI H$_2$O to give a yield of 91%. ^{1}H NMR 600 MHz (DMSO-d$_6$): δ 6.8 4H ddd, δ 7.4 4H ddd, δ 7.5–7.6 2H dddd, 2H dddd, 1H tt, δ 10.2 2H s. ^{31}P NMR 600 MHz (DMSO-d$_6$): δ 25.1 1P s (Figure S2).

Synthesis of bis-4-Glycidylethertriphenylphosphine Oxide (bGE-tPPO). To a 1000 mL three-neck round-bottom flask equipped with a mechanical stirrer, refluxing condenser, addition funnel, and N$_2$ inlet/outlet, 4,4-BH-tPPO (51.85 g, 0.17 mols, 1 eq.) was charged with epichlorohydrin (629.14 g, 6.8 mols, 40 eq.) and 30% benzyltrimethylammonium chloride in methanol and heated to 70 °C for 27 h with moderate stirring. The intermediate was concentrated using reduced pressure. The intermediate was dissolved in 225 mL of 1,2-dichloroethane and 18% NaOH (13.6 g, 0.34 mols, 2 eq.) in DI H$_2$O and saturated Na$_2$CO$_3$ was added dropwise at a rate of two drops per second. The temperature of the reaction was then increased to 75 °C and the mixture was stirred vigorously for 5 h and then cooled to ambient temperature. The product was then washed eight times with DI H$_2$O and concentrated using reduced pressure to give a yield of 89% (HCC = 0.064 wt %; EEW = 230.97 g/eq). ^{1}H NMR 600 MHz (DMSO-d$_6$): δ 6.8 4H ddd, δ 7.4 4H ddd, δ 7.5–7.6 2H dddd, 2H dddd, 1H tt, δ 10.2 2H s. ^{31}P NMR 600 MHz (DMSO-d$_6$): δ 25.0 1P s (Figure S3).

Epoxidation of the resultant bisphenol afforded the desired bGE-tPPO monomer with a high yield (89%). Precautionary measures were taken to not heat the monomer higher than 90 °C because homopolymerization was observed at higher temperatures.

Diamine Monomer Synthesis. bA-tPPO was synthesized according to a literature procedure with some modification (Scheme 2).[25] The details are as follows.

Synthesis of bis-3-Nitrotriphenylphosphine Oxide (3,3-Bn-tPPO). To a 1000 mL three-neck round-bottom flask equipped with a magnetic stirrer, reflux condenser, addition funnel, and N$_2$ inlet/outlet, triphenylphosphine oxide (45.1 g, 0.162 mol, 1 eq.) and 200 mL of 96% sulfuric acid were added. The reagent was dissolved with vigorous stirring, and the reaction system was cooled to −5 °C. A solution of fuming nitric acid (20.35 g, 0.323 mol, 2 eq.) in sulfuric acid (200 mL) was added dropwise, with care being taken to not allow the reaction to exceed 0 °C during addition. Care was taken to maintain a slow addition rate of dilute nitric acid to minimize the formation of mono- and tri-substituted intermediates. The reaction mixture was stirred and allowed to react for 8 h. The reaction mixture was then hydrolyzed over ice, extracted with chloroform, and washed with 3 M NaOH solution until neutralized. The solution turned orange upon addition of NaOH. The solution was then concentrated using reduced pressure and recrystallized from absolute ethanol to

Scheme 2. Synthesis of bis-3-Nitrotriphenylphosphine Oxide (3,3-BN-tPPO) and bis-3-Aminotriphenylphosphine Oxide (bA-tPPO)
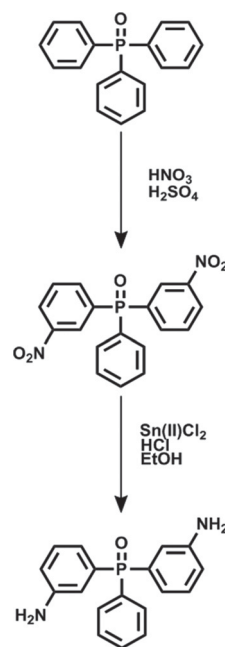
give a yield of 67%. ^{1}H NMR 600 MHz (DMSO-d$_6$): δ 7.6 2H ddd, δ 7.75 2H dddd, 1H tt, δ 7.8 2H dddd, δ 8.2 2H ddd, δ 8.45 2H dt, δ 8.65 2H ddd. ^{31}P NMR 600 MHz (DMSO-d$_6$): δ 25.1 1P s (Figure S4).

Synthesis of bis-3-Aminotriphenylphosphine Oxide (Ba-tPPO). A 500 mL three-neck round-bottom flask equipped with a magnetic stirrer and N$_2$ inlet/outlet was charged with 3,3-BN-tPPO (10 g, 0.03 mol, 1 eq.) and anhydrous tin(II)chloride (90 g, 0.475 mol, 16 eq.). A solution of 100 mL of fuming hydrochloric acid in 200 mL of absolute ethanol was introduced into the flask and stirred at ambient temperature for 5 h. The solution was then concentrated under reduced pressure, neutralized with 25% aqueous NaOH solution, redissolved in ethanol, and filtered through celite to remove tin(II)chloride. The filtered product was extracted with chloroform, washed three times with deionized water, and concentrated to give a pure product with 95% yield. Purification of the product required repeated extraction of the aqueous layer with an organic solvent due to the high solubility of bA-tPPO in water. ^{1}H NMR 600 MHz (DMSO-d$_6$): 4H δ 5.45 4H dd, δ 6.6 2H ddd, δ 6.7 2H ddd, 1H tt, δ 6.8 2H ddd, δ 7.2 2H ddd, δ 7.5 2H dddd, δ 7.55 3H m. ^{31}P NMR 600 MHz (DMSO-d$_6$): δ 25.2 1P s (Figure S5). Alternate approaches to reduce 3,3-BN-tPPO have been reported in the literature using a more easily removable Pd catalyst.[26] However, the published procedure utilized a hydrogenation apparatus at elevated temperatures, which may not be readily accessible.[26]

Monomer Characterization. Nuclear magnetic resonance (NMR) spectroscopy was conducted on a Bruker Ascend 600 MHz spectrometer for ^{1}H NMR and ^{31}P NMR with tetramethylsilane as an internal standard. Fourier transform infrared spectroscopy (FTIR) was carried out on a PerkinElmer Frontier spectrometer with the scanning wavenumber in the range of 400−4000 cm^{-1} at 32 scans.

Thermomechanical Sample Preparation and Characterization. Epoxide-amine slurries with statistically varying phosphorus concentrations (Table 1) were heated to 120 °C and degassed for approximately 30 min prior to polymerization in a programmable oven. The temperature profile for polymerization was performed as follows: ramp from 120 to 180 °C at a rate of 1 °C·min^{-1} and isothermal hold at 180 °C for 3 h. Samples containing bA-tPPO were prepared via a solvent-based method via a solvent-based method described as follows. The epoxide and diamine were dissolved in a minimum necessary amount of ethanol and then concentrated. The

Table 1. Composition of Prepared Epoxy-Amine Polymers

sample identity	epoxide/amine identity	sample molar ratios	calculated[a] [P] (wt %)	experimental[b] [P] (wt %)
0−PPO	------------:TGDDM:3,3-DDS:-----------	----:1.0:1.0:---	0.00	0.00 ± 0.00
20−PPO	bGE-tPPO: TGDDM: 3,3-DDS:-----------	1.0:2.0:2.5:---	1.64	1.18 ± 0.07
40−PPO	bGE-tPPO:TGDDM:3,3-DDS:-----------	2.0:1.0:2.0:---	3.51	3.08 ± 0.02
66−PPO	bGE-tPPO:-----------:3,3-DDS:-----------	2.0:----:1.0:---	5.67	5.41 ± 0.08
100−PPO	bGE-tPPO:-----------:----------:bA-tPPO	2.0:----:---:1.0	8.06	7.78 ± 0.11

[a]Theoretical values calculated from empirical formulas of polymer structures. [b]Experimental determination from surface XPS survey data.

Table 2. Thermal Behavior of Prepared Phenylphosphine Oxide Epoxies

sample identity and [P] (weight %)	$T_{5\%}$[a] (°C)	$C_{600°C}$[b] (wt %)	$C_{800°C}$[c] (wt %)	T_g[d] (°C)
------------/DGEBA−3,3 DDS	403.3 ± 1.3	28.1 ± 0.2	1.4 ± 1.7	157.9 ± 1.0
0−PPO/TGDDM−3,3 DDS	343.4 ± 0.7	38.9 ± 0.7	0.8 ± 0.5	233.0 ± 0.3
20−PPO/1.6 wt % P	336.8 ± 1.5	40.8 ± 1.2	4.9 ± 2.0	219.0 ± 0.6
40−PPO/3.5 wt % P	337.3 ± 1.3	41.4 ± 0.9	13.6 ± 1.9	212.5 ± 4.4
66−PPO/5.7 wt % P	355.0 ± 1.5	44.0 ± 2.0	24.1 ± 6.2	204.9 ± 1.0
100−PPO/8.1 wt % P	348.0 ± 5.1	43.8 ± 0.5	25.1 ± 2.7	201.9 ± 1.0

[a]Temperature of 5 weight % loss. [b]Char yield at 600 °C. [c]Char yield at 800 °C. [d]Glass transition temperature.

clarified epoxide-amine prepolymer was then cast into a mold, degassed, and polymerized as previously described. Thermal analyses were performed using a TA instruments Q50 thermogravimetric analysis (TGA) instrument at a heating rate of 10 °C·min^{-1} with the temperature ranging from 25 to 800 °C in air, in triplicate. Dynamic mechanical analyses (DMA) were performed using a TA instruments Q800 DMA in a multifrequency strain mode using a film tension clamp, in triplicate. Temperature ramp tests were performed at an oscillation amplitude of 15, a static force of 0.01 N, a force track of 125%, and a sampling interval of 2 pts·s^{-1} from room temperature to 300 °C at a heating rate of 3 °C·min^{-1}. T_g values were obtained from the peak of the obtained tanδ curve. Sample sizes were kept constant at approximately 20 mm · 5 mm · 1 mm (l · w · h).

Cleaning of Silicon Wafers. Silicon wafers were cut into 1.5 cm × 1.5 cm pieces and cleaned using the Radio Corporation of America (RCA) procedure to remove organic residues and oxidize the surface of the wafer. The general recipe for RCA cleaning is five parts deionized (DI) water, one part 27% ammonium hydroxide, and one part 30% hydrogen peroxide. DI water and ammonium hydroxide were added to a beaker and heated to 70 °C for 5 min, and then the beaker was removed from heat and hydrogen peroxide was added. The silicon wafers were transferred to the beaker and heated at 70 °C for 15 min. After 15 min, the wafer was removed from the solution and washed multiple times with DI water. Clean substrates were stored in an oven at 120 °C before film spin-casting.

Thin-film Preparation. Epoxide-amine solutions with statistically varying phosphorus concentrations were prepared at concentrations of 0.15 g·mL^{-1} in acetone (Table 1). Solutions containing bA-tPPO were prepared using ethanol. All solutions were filtered through a filter pipette to remove particulate matter prior to spin-casting. Five drops of solution were deposited on prepared wafers and spin-cast at an acceleration of 2002 rpm·s^{-1} with a top speed of 2000 rpm for 60 s.

The spin-cast films were dried at ambient conditions for 120 min followed by drying under reduced pressure at an ambient temperature for 120 min. Thin films were cured at 80 °C for 48 h, and curing was monitored using FTIR spectroscopy by observing the disappearance of epoxide peaks (912 cm^{-1}).

Thin-film Characterization and Atomic Oxygen Exposure. The AO exposure test was performed using a Diener zepto radio frequency reactive ion etcher equipped with ultra high purity grade oxygen gas. AO fluence was calculated based on the mass loss of a reference Kapton H polyimide using eq 1

$$F = \frac{m}{\rho A E} \tag{1}$$

where F is the total AO fluence (O atoms·cm^{-2}), m is the mass loss of Kapton (g), ρ is the density of Kapton (1.42 g·cm^{-3}), A is the surface

area of the exposed Kapton sample (cm^2), and E is the erosion constant of Kapton (3·10^{-24} cm^3·O atom^{-1}).

Atomic oxygen exposure was performed in the following cumulative time increments: 1, 2, 3, 4, 5, 10, 15, 20, 25, 30, and 60 min. The thin-film thickness was analyzed in triplicate after each incremental exposure. Thin-film thickness measurements were performed using a Filmetrics interferometer with a refractive index of n = 1.45.

Thin films containing 0 and 1.6 wt % phosphorus did not retain sufficient structural integrity to quantify their thicknesses beyond a 20 minute (9.6·10^{20} O atoms·cm^{-2}) exposure and were entirely eroded after a 60 minute exposure. Therefore, concurrently exposed macroscopic samples of dimensions 20 mm · 5 mm · 1 mm (l · w · h) were used for AFM-IR and XPS characterization.

The cumulative AO fluence received was compared to an equivalent duration in orbit as a means to understand the relative magnitude of the AO exposure performed in this study based on the data from a mission on the International Space Station (ISS) launched on June 2001, when the sun entered a period of high activity. The total AO exposure during this period was quantified to be 3.28·10^{21} O atoms·cm^{-2} for 1 year of exposure.[20,27]

Film Surface Characterization. *X-ray Photoelectron Spectroscopy.* XPS experiments were conducted using a ThermoFisher ESCALAB Xi+ spectrometer equipped with a monochromatic Al X-ray source (1486.6 eV) and a MAGCIS Ar$^+$/Ar$_n^+$ gas cluster ion sputter gun. Measurements were performed using the standard magnetic lens mode and charge compensation. The base pressure in the analysis chamber during spectral acquisition was 3·10^{-7} mBar. Spectra were collected at a takeoff angle of 90° from the plane of the surface. The pass energy of the analyzer was set at 150 eV for survey scans with an energy resolution of 1.0 eV; the total acquisition time was 220 s. Binding energies were calibrated with respect to C 1s at 248.8 eV. Sputter depth profiling was performed by rastering an argon ion beam in the cluster mode (6 keV, Ar$_{300}^+$) over a 2 mm^2 area at an angle of 30° to the sample normal. To avoid crater edge effects, an X-ray spot size of 650 μm was employed. The X-ray gun was blanked during each argon sputtering step to minimize changes in composition due to X-ray exposure. All spectra were recorded using Thermo Scientific Advantage software; data files were translated to VGF format and processed using the Thermo Scientific Advantage package v5.9904.

Atomic Force Microscopy−Infrared Spectroscopy. AFM-IR spin-cast films before and after exposure to an AO flux equivalent to 2.88·× 10^{21} atoms·cm^{-2} were imaged using a nanoIR3 AFM-IR from Bruker Instruments (Santa Barbara, CA) coupled to an MIRcat-QT quantum cascade, mid-infrared laser (frequency range of 917−1700 cm^{-1} using a pulse repetition rate of 1470 kHz). AFM-IR data were collected in

the tapping mode using a gold-coated AFM probe (spring constant (k): 40 N/m and resonant frequency (f_o): 300 kHz) manufactured by Bruker. The pulsed, mid-IR laser was tuned to frequencies unique to each component as determined by FTIR characterization. The acquired images were further processed using Analysis Studio software.

■ RESULTS AND DISCUSSION

Thermal Properties of PPO Epoxy-Amines. The glass transition temperatures (T_g) and thermal stabilities of the prepared polymers were measured by DMA and TGA as reported in Table 2. The influence of the bGE-tPPO monomer on polymer T_g and thermal stability is observed through the comparison to an epoxide monomer with similar functionality (DGEBA) and a diamine monomer with similar structure and isomerism (3,3-DDS). Further comparison with the high-performing TGDDM epoxide monomer highlights the excellent thermal behavior of the prepared PPO epoxide and diamine monomers.

Epoxy-amines prepared using DGEBA−3,3 DDS and TGDDM−3,3 DDS were found to exhibit T_gs of 158 and 233 °C, respectively. Replacement of DGEBA with a stoichiometric equivalent of the bGE-tPPO monomer (samples DGEBA−3,3 DDS and 66−PPO, respectively) was found to increase the resultant polymer T_g by 47 °C (158 and 205 °C, respectively). Subsequently, the effect of the bA-tPPO monomer on epoxy-amine T_g was compared to a stoichiometric equivalent of the 3,3-DDS monomer (samples 100−PPO and 66−PPO, respectively). The observed T_g values differed by only 3 °C. Based on these results, it was concluded that epoxide monomers with a backbone triphenylphosphine oxide moiety (bGE-tPPO) significantly increased polymer T_g relative to bisphenol-A-based epoxide monomers (DGEBA). Furthermore, the effect of diamine monomers with triphenylphosphine oxide backbone moieties on polymer T_g appears to be similar relative to a sulfone moiety, as evidenced by the similar T_g values when comparing bA-tPPO to 3,3-DDS.

The effect of bGE-tPPO on epoxy-amine T_g was further analyzed via comparisons to the high-performing epoxide monomer TGDDM. Epoxy-amines based on TGDDM and 3,3-DDS monomers are commonly used in rigorous aerospace applications and serve as the benchmark chemistry for the remainder of this work. It was found that epoxy-amines prepared using the difunctional bGE-tPPO monomer exhibited a 32 °C lower T_g compared to that of tetrafunctional TGDDM (66−PPO and 0−PPO, respectively). In contrast, the DGEBA−3,3 DDS epoxy-amine's T_g was 75 °C lower than that of TGDDM−3,3 DDS. Crucially, the prepared PPO epoxy-amines retained a T_g above 200 °C, confirming their suitability for high-temperature applications.

Interestingly, the onset of thermal degradation and char yield at 600 °C in air of PPO epoxy-amines exhibited almost no change with the increasing PPO content (Table 2; Figure S6). The obtained thermograms demonstrated a relatively consistent $T_{5\%}$ at approximately 340 °C regardless of the PPO content. The onset of degradation at 340 °C occurs due to the thermal degradation of the alkyl epoxy bonds, which is not expected to be influenced by the addition of PPO.[28] Furthermore, the obtained char yields at 600 °C ranged from 40.8 wt % for 20−PPO to 43.8 wt % for 100−PPO. However, at 800 °C, an increase in the char yield corresponding to the increased initial [P] was observed, ranging from 4.9 wt % for 20−PPO to 25.1 wt % for 100−

PPO. Previous literature study on the incorporation of phosphorus into polymers suggests an increase in the high-temperature char yields of resultant polymers through the formation of a phosphate-based char.[22] The observed results were therefore in good agreement with the literature precedent regarding the thermal stability of PPO compounds.[22]

Atomic Oxygen Resistance of PPO Epoxy-Amines. Technical details regarding AO exposure using oxygen plasma etchers and their applicability to LEO conditions have recently been discussed by Banks et al.[29] The prepared samples were exposed to a total fluence of 2.88×10^{21} O atoms·cm^{-2} in incremental exposures for a cumulative exposure time of 60 min; the thin-film thickness was assessed after each incremental exposure. Film thickness as a function of AO exposure time is shown in Figure 3a. Thin films containing 0
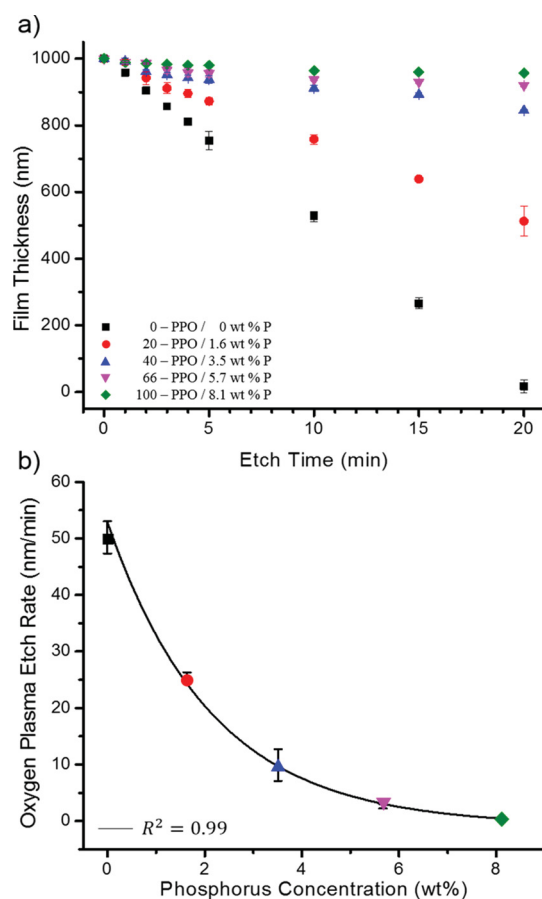

Figure 3. (a) PPO epoxy-amine thin-film surface erosion during AO exposure; 20 min etch time equivalent to approx. 1×10^{21} O atoms·cm^{-2} and (b) dependence of [P] on erosion rate fitted with an exponential line of best fit[a] ([a]Oxygen plasma etch rate value is obtained from the slope of linear fit for the final 3 film thicknesses; the best fit curve is calculated using the OriginPro 8.5 software).

and 1.6 wt % phosphorus did not retain sufficient structural integrity to quantify their thicknesses beyond a 20 minute (9.6×10^{20} O atoms·cm^{-2}) exposure and were entirely eroded after a 60 minute exposure. For this reason, Figure 3a ends at a cumulative AO exposure time of 20 min; the complete data set is shown in Figure S7.

All samples demonstrated a loss in film thickness upon AO exposure (Figure 3a); however, samples containing PPO exhibited nonlinear erosion rates consistent with previous

Table 3. XPS Surface Analyses of Prepared Thin Films before and after Exposure to an AO Flux Equivalent to 2.88×10^{21} O Atoms·Cm$^{-2 a}$

calculated [P][b] (wt %)	unexposed surface atomic weight %			exposed surface atomic weight %		
	O1s	C1s	P2p	O1s	C1s	P2p
0 wt % P	32.5 ± 0.6	59.1 ± 0.5		40.1 ± 0.7	47.2 ± 0.3	
1.6 wt % P	28.1 ± 0.7	63.2 ± 1.1	1.2 ± 0.1	40.0 ± 0.9	38.5 ± 0.9	11.6 ± 0.8
3.5 wt % P	28.0 ± 0.1	60.4 ± 0.1	3.1 ± 0.0	35.3 ± 0.1	45.6 ± 0.3	11.4 ± 0.3
5.7 wt % P	24.5 ± 0.1	64.2 ± 0.1	5.4 ± 0.1	38.3 ± 0.3	39.4 ± 0.3	16.0 ± 0.2
8.1 wt % P	23.6 ± 0.1	66.3 ± 0.2	7.8 ± 0.1	39.7 ± 0.6	41.1 ± 0.9	14.6 ± 0.3

[a]Compositions obtained from surface XPS survey data (Figure S8). [b]Calculation based on the empirical formula of the polymer structure.

literature reports.[30] Based on the results shown in Figure 3a, it is clear that the rate of AO erosion of epoxy-amines rapidly decreases with increasing PPO addition, with dramatic reductions in AO erosion achieved above 5 wt % P. This suggests that a minimum of 5 wt % P is necessary to observe significant resistance to AO degradation. Increasing [P] to 8.1 wt % further improved the AO resistance 100-fold relative to 0−PPO after a cumulative 60 minute AO exposure (2.88×10^{21} O atoms·cm^{-2}).

Figure 3b provides insight into the concentration dependence of P on the oxygen plasma etch rate of the resultant epoxy-amine. Importantly, increasing [P] resulted in significantly reduced erosion rates, with an exponentially decaying trend observed between initial [P] and the oxygen plasma etch rate. The observed trend is consistent with reports on AO passivation in PPO-containing polymers.[30] Furthermore, the trend reported herein is consistent with observations reported by Lei et al. regarding the AO erosion of Si-containing polymers.[31] It is expected that Si- and P-containing polymers exhibit similar mechanisms of AO resistance and therefore observations in these materials are somewhat comparable. There are a few possible causes for the trend observed in Figure 3b. It is expected that the surface coverage of the PPO moiety increases with the increasing PPO content, which would result in a more complete PO$_x$ passivation layer and less severe oxidative degradation of the remaining organic portions of the polymer. Furthermore, it is hypothesized that increasing PPO content results in a denser and more homogenous PO$_x$ passivation layer, resulting in an improved passivation effect. However, the effect of increasing [P] on AO resistance is expected to plateau as the formed passivation layer approaches an optimal composition to resist AO erosion. Based on these results, it is evident that epoxy-amines with high PPO concentration have high resistance to AO in the simulated AO environment, and that passivation efficacy is dependent on [P].

It is worth noting that the AO erosion rate of polymers also depends on the composition of the organic components, where aliphatic compounds degrade more readily than aromatic compounds. Therefore, although the precise erosion rates of PPO-containing polymers relative to [P] will vary slightly from the reported trend depending on the polymer structure, the observed AO erosion rate trend as a function of [P] is expected to broadly hold true.[16,30]

Surface Analysis and Morphology. Samples were analyzed by XPS to determine the effects of AO exposure on surface atomic composition, with the results of the XPS survey spectra reported in Table 3. The calculated [P] values based on polymer formulation for samples prior to AO exposure agreed with the experimentally obtained [P] values, giving confidence in the obtained results. After exposure to AO, the concentration of C decreased in agreement with previous literature results.[30] This decrease is due to the oxidation of carbon-based moieties, where the final product is often a volatile compound. A corresponding increase in [O] was observed in all samples as expected from oxidation by AO. In PPO-containing samples, an increase of [P] up to a maximum of 16.0 wt % was observed after AO exposure, indicative of passivation layer formation. Interestingly, there is no clear trend with regard to surface [P] after AO exposure and AO shielding efficacy, and the low standard deviation implies a high degree of precision in the results. This suggests that the surface [P] atomic composition does not necessarily correlate with the PO$_x$ passivation layer performance. However, it remains a useful metric to confirm the PO$_x$ passivation layer formation.

Surface morphology analyses were performed using AFM-IR, and the results are shown in Figure 4. Scans of the prepared epoxy-amine thin films without incorporated PPO are shown in Figure S9. AFM-IR scans of PPO-containing samples show smooth and homogenous film surfaces before AO exposure (Figure 4a; Figure S10). Root mean square (RMS) analyses were performed to quantify the observed differences in height, and the results are summarized in Table 4. The reference peak used to IR-scan the surfaces was the phosphorus to phenyl bond (P−Ph) observed at 1438 cm^{-1}. This peak was chosen for its good separation from other peaks (Figure S11) and its expected disappearance when the phosphine oxide moiety oxidizes into the PO$_x$ passivation layer as reported in the literature.[32]

Surface scans of samples before AO exposure show smooth and homogenous sample surfaces across all prepared samples. The RMS roughness for all samples before AO exposure did not exceed 0.3 nm, indicating excellent surface smoothness (Table 4). Likewise, phase scans of exposed samples provided further insight into the surface morphology of the formed PO$_x$ passivation layer. The obtained phase diagrams provide clearer images which allow for further qualitative analysis of the passivation layer. The prepared epoxy-amines with low [P] (20−PPO) exhibited large nodelike structures after AO exposure, where the structure phase was observed to be heterogenous with respect to the center and edges, as observed in sample 0−PPO. Additionally, microcracks and crevasses were clearly distinguishable in the phase image of sample 20−PPO after AO exposure. As the [P] content increased to 40−PPO, the formed nodelike structures appeared to decrease in size and formed a more regular surface, although cracks and crevasses between nodes remained apparent. Upon further increasing [P] to 66−PPO, the size of the observed nodes did not appear to change; however, no crevasses were observed in the obtained images. This change indicates a more complete formation of the passivation layer as a function of increasing
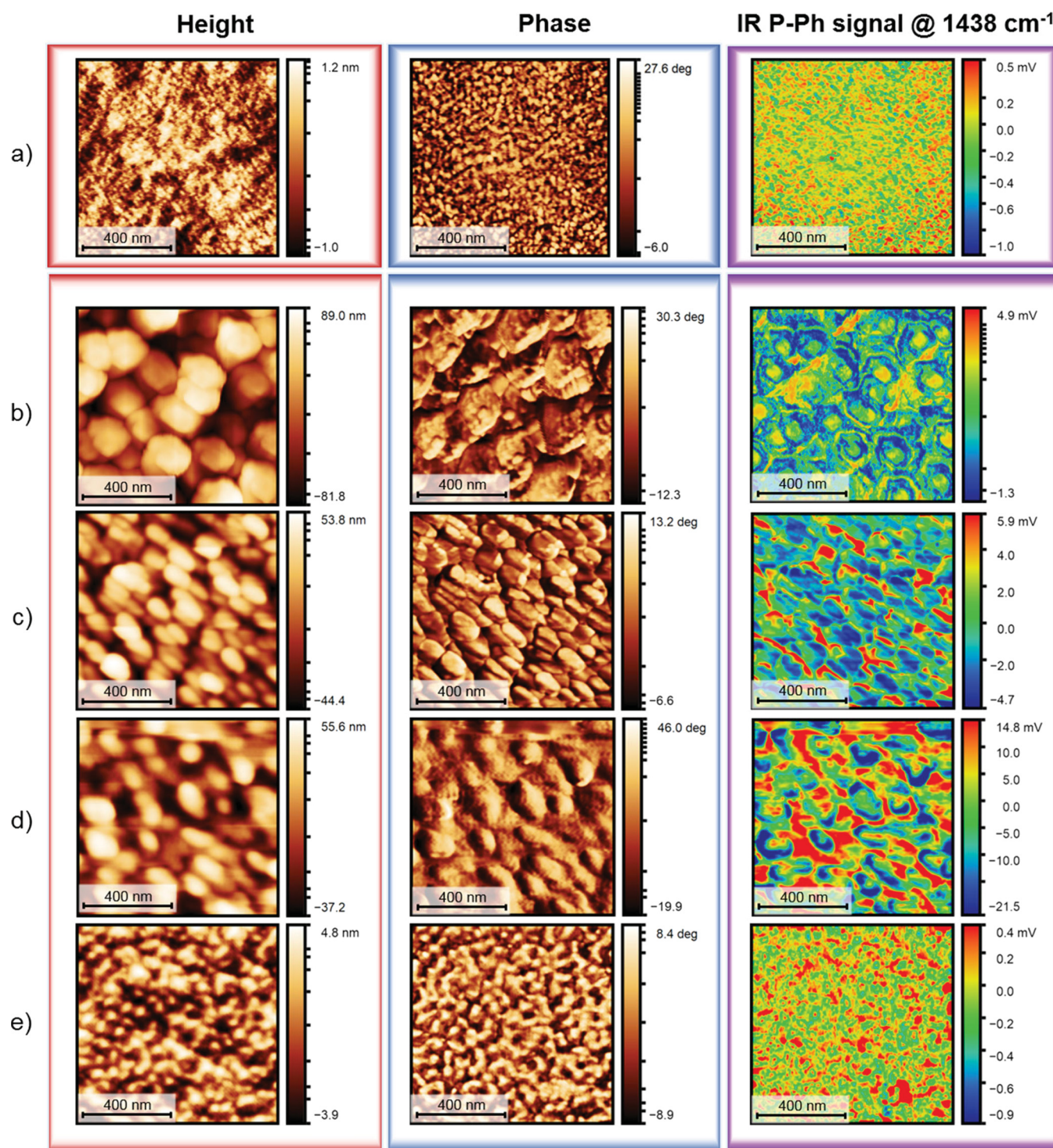
Figure 4. AFM-IR images of spin-cast thin films before (a) and after (b−e) exposure to an AO fluence equivalent to 2.88×10^{21} atoms·cm^{-2} (a) height, phase, and IR map of 40−PPO; (b) height, phase, and IR map of 20−PPO; (c) height, phase, and IR map of 40−PPO; (d) height, phase, and IR map of 66−PPO; and (e) height, phase, and IR map of 100−PPO.

[P] with implications on AO diffusion to be discussed in the later portion of this work. At high [P] (100−PPO), the observed passivation layer appeared to be well-formed, with no apparent crevasses or cracks. Scans measuring relative variation in P−Ph IR signal strength of polymer film surfaces after AO exposure provide key insights into the composition of the formed passivation layers as a function of [P]. Generally, a trend of decreasing deviation in the P−Ph signal was observed

as [P] increases. The sample 100−PPO deviated from this trend with an observed deviation of ± 0.8 mV, indicating a relatively homogenous distribution of the P−Ph signal unique to the prepared epoxy-amines with >8 wt % P.

Furthermore, the distribution of the P−Ph signal around the observed nodes provides some insight into the chemical composition of the nodes. The observed node structures in samples with low [P] demonstrate two distinct concentrations

Table 4. Root Mean Square (RMS) Values of Thin-Film Surface Heterogeneities before and after AO Exposure[a]

AO flux (O·atoms·cm^{-2})	thin-film height RMS (nm)				
	0−PPO	20−PPO	40−PPO	66−PPO	100−PPO
0	0.2	0.2	0.3	0.2	0.2
2.88·× 10^{21}	1.4	27.5	14.1	14.2	1.4

[a]RMS values are calculated using statistical quantities function embedded in Gwyddion software.

of the P−Ph bond. Areas with relatively lower [P−Ph] appear to be distributed around the extremes of the node structures, with areas of relatively higher [P−Ph] appearing in the center of the observed nodes. To the best of the author's knowledge, the penetration depth of AFM-IR remains poorly understood; however, it is plausible that the spectrometer detected unoxidized material at some depth beneath the passivation layer. Importantly, the strength of the signal appears to be insufficient to detect unoxidized polymer at the edges of the nodes. These heterogeneities suggest a gradient of composition in the imaged nodes. These observations remain consistent across all samples, with a large decrease in the observed node size between samples 66−PPO and 100−PPO. This is attributed to the significantly more homogenous passivation layer formation observed in the high [P] sample with a relatively homogenous phase behavior. Finally, IR mapping of samples showed a homogenous dispersion of the P−Ph bond with small deviations ($\pm$ 0.5 mV) across most samples, where mV is indicative of the relative concentration of the IR peak of interest. Sample 100−PPO did demonstrate a deviation of $\pm$

1.5 mV; however, this is not anticipated to be significant as the distribution of the signal was homogenous and an increase in signal is possible due to the higher [P] in the polymer.

All samples exhibited significant surface roughening and more heterogenous surface morphology after exposure to an AO flux equivalent to 2.88×10^{21} O atoms·cm^{-2} (Figure 4). The epoxy-amine polymer with no [P] shown in Figure S7 demonstrated a somewhat smooth scalelike surface with an RMS of 1.4 nm (approximately 7x greater than before AO exposure). This likely occurred due to homogenous removal of organic matter during AO exposure as opposed to PPO-containing epoxy-amines. In contrast, the surfaces of epoxy-amines with PPO in the polymer backbone are smoother with a more homogenous phase behavior. Furthermore, the RMS follows a decreasing trend with increasing [P], from 27.5 to 1.4 nm. The greatest differences in measured RMS were observed between samples 20−PPO and 40−PPO (27.5 nm and 14.1 nm, respectively) and samples 66−PPO and 100−PPO (14.2 nm and 1.4 nm, respectively). These results suggest that epoxy-amines with increasing P content become increasingly resistant to AO attack, corresponding to the decreasing thin-film thickness loss illustrated in Figure 3. Crucially, the observed trend of decreasing RMS with increasing [P] is consistent with literature reports of the SiO$_x$ passivation layer behavior in response to AO exposure.[31,33] To the best of the authors' knowledge, no such observations have been reported regarding PO$_x$ passivation layers to date. A noteworthy example is Lei et al.'s work wherein it was observed that a polyimide sample containing 8.8 wt % POSS exhibited an RMS of 112.6 nm after exposure to an AO flux of 3.87×10^{20} O atoms·cm^{-2}, whereas
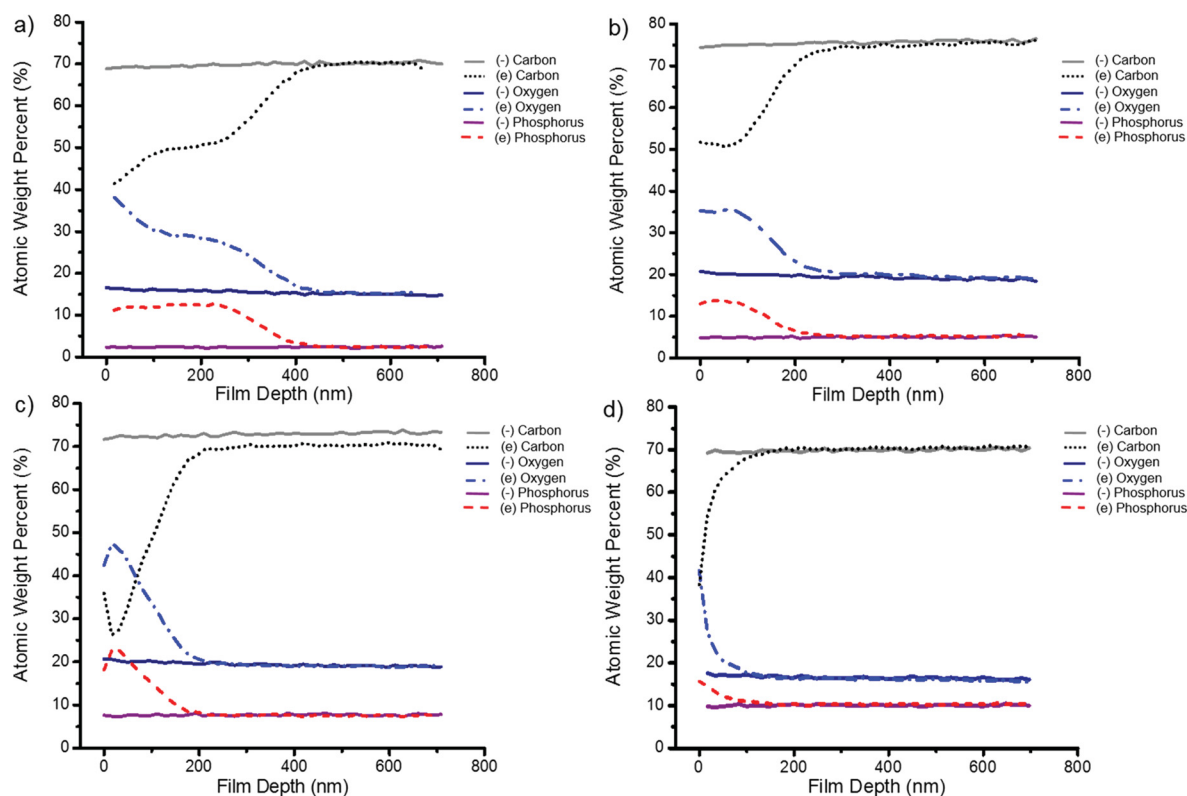

Figure 5. Compiled XPS depth profiles of PPO epoxy-amines depicting weight percent of select atomic species before (−) and after (e) exposure to an AO flux equivalent to 2.88×10^{21} O atoms·cm^{-2} (a) XPS depth profile of 20−PPO, (b) XPS depth profile of 40−PPO, (c) XPS depth profile of 66−PPO, and (d) XPS depth profile of 100−PPO.
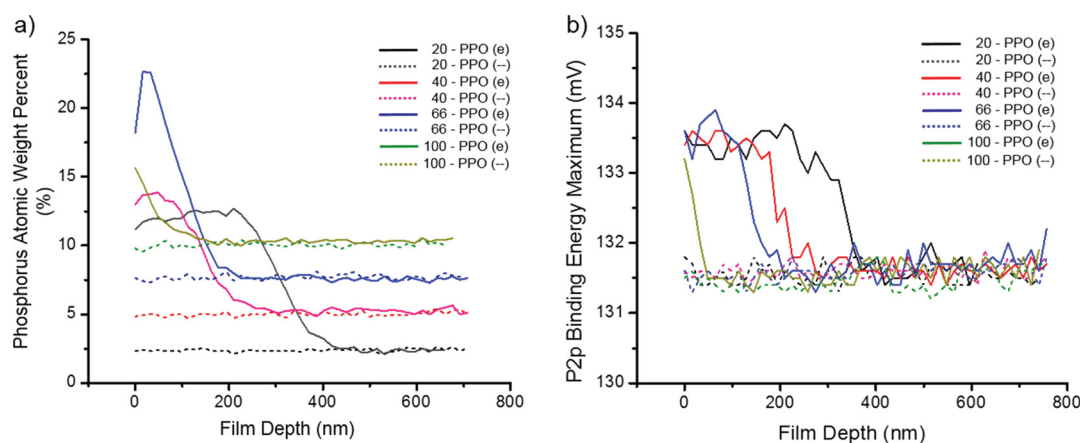
Figure 6. (a) Summary of P XPS depth profiles of PPO epoxy-amines before (−) and after (e) exposure to an AO flux equivalent to 2.88×10^{21} O atoms·cm^{-2}. (b) Overlaid P2p binding energy peak maxima[a] as a function of film depth before (−) and after (e) exposure to an AO flux equivalent to 2.88×10^{21} O atoms·cm^{-2} ([a]Values obtained from high-resolution P2p spectra depth profiles of PPO epoxy-amine thin films (Figures S12 and 13)).

a sample containing 21.9 wt % POSS exhibited an RMS of 7.3 nm after exposure to the same AO flux.[31]

Thin-film Depth Profiling. Epoxy-amines with PPO moieties in the backbone were analyzed via XPS depth profiling after exposure to an AO flux equivalent to 2.88×10^{21} O atoms·cm^{-2}, and the results are shown in Figure 5. Oxidation of polymer films by AO results in rapid gasification of C-based moieties and leads to significant mass loss. These oxidation reactions also result in changes to the atomic stoichiometry of the remaining material as a function of film depth. The depth behavior of these oxidation reactions is therefore observed by monitoring [C], [O], and [P] as a function of film depth. Importantly, the illustrated polymer atomic compositions as a function of film depth were interpreted starting from the pristine atomic composition occurring at approximately 800 nm moving toward the surface composition at 0 nm. In this way, the atomic composition of the polymer was evaluated as it approached PO$_x$ passivation layer formation and volatilization. It can be observed that samples that did not experience AO exposure (indicated by solid lines in Figure 5) maintained consistent [C], [O], and [P] over the depth of the film. In contrast, PPO epoxy-amines that experienced AO flux demonstrated a series of oxidative transitions over the depth of the film, with a clear variation in the number of transitions and depth of oxidative degradation corresponding to differences in initial [P].

The prepared epoxy-amines with low [P] (20−PPO) exhibited two oxidative transition events at approximately 0−100 nm and approximately 250−400 nm (Figure 5a). The first event, located at approximately 0−100 nm, is the gradient transition to the ultimate oxidative state of the film prior to surface erosion. This is hypothesized to be the region wherein the formed PO$_x$ passivation layer no longer effectively protects the underlying polymer. The second oxidative transition event occurring at approximately 250−400 nm is the gradient transition to the pristine composition of the film. This is expected to be the region of the polymer film wherein the generated PO$_x$ passivation layer does not prevent AO from reacting with readily oxidizable moieties such as alkyl groups. The analyzed sample further exhibited a "steady-state" region at approximately 100−300 nm wherein no significant changes in atomic concentration were observed. This is hypothesized to be the region of the polymer film where the readily oxidizable

moieties have been exhausted and the PO$_x$ passivation layer protects the underlying material from the inbound AO. Interestingly, the gradient transition occurring at approximately 0−100 nm appears to be independent of [P], implying that this gradient transition does not result in further changes to the PO$_x$ portion of the passivation layer. The cumulative gradient transitions of phosphorus to the original concentration are considered to be representative of the thickness of the passivation layer for the remainder of this work.

As [P] increases to 40−PPO (Figure 5b), a single gradient transition is observed, occurring between approximately 100−250 nm. This gradient transition is expected to be similar to that in the region of 250−400 nm in sample 20−PPO. Further increasing the [P] to 66−PPO (Figure 5c) shifts this gradient transition nearer to the surface of the film, from 30−175 nm. These results suggest that increasing [P] improves the formed PO$_x$ passivation layer and limits the depth of diffusion of AO into the polymer. Interestingly, another gradient was observed in sample 66−PPO that replicated three times, confirming the validity of the observed anomaly. The observed transition occurring between 0−25 nm shown in Figure 5c includes a loss of [P] and [O] and a rise in [C], as measured from a depth of 25 nm to the surface of the polymer film (0 nm). This is an opposite trend expected from the formation of a PO$_x$ passivation layer. Instead, it is hypothesized that this gradient transition is indicative of atomization of the passivation layer as a response to surface AO reactions. Comparing [P] as a function of film depth across all samples reveals that this observation is consistent in samples 20, 40, and 66 PPO as evidenced by decreases in [P] within 50 nm of the film surface (Figure 6a). The PPO epoxy-amine with the highest [P] (100−PPO) was not observed to experience atomization as measured by XPS depth profiling due to a lack of [P] loss at the surface of the film. However, the continuous film height loss measured by interferometry during AO exposure suggests that atomization did occur. It is expected that all polymers with inorganic components included to improve AO resistance will undergo some degree of atomization as the continued erosion of organic polymer components will induce critical structural failures within the passivation layer. More complete formation of the passivation layer (corresponding to higher initial inorganic concentrations) is anticipated to reduce the rate of

atomization—leading to the differences in AO erosion rates reported in Figure 3b.

Further differences in the passivation layer behavior can be observed from the magnitude of the gradient transition occurring within the deepest portions of the film. In sample 20–PPO, this transition is observed to occur between 250–400 nm (Figures 5 and 6a). Generally, the film depth of this transition follows a decreasing trend as [P] increases and is likely related to the rate and density of formation of the passivation layer. This suggests that the formed passivation layer is more effective at preventing AO diffusion into the polymer with increasing [P]. This is further confirmed through the obtained AFM-IR images shown in Figure 4 wherein at approx. 5 wt % P, cracks and crevasses cease to appear within the passivation layer due to a sufficiently high [P] in the formulation. Finally, the obtained [P] depth profiles give a clear insight into the thickness of the formed phosphate passivation layer. In samples with low [P] (20–PPO), the fully formed passivation layer is observed between 0 and approximately 250 nm; as [P] increases, the fully formed layer is observed to decrease in thickness significantly. At the highest measured [P], no steady state of [P] was observed, suggesting a passivation layer thickness too thin to be detectable through the means used in this work. High-resolution P2p spectra of the AO-exposed films provide further insight into the oxidative reactions occurring with PPO throughout the depth of the polymer.

A summary of the high-resolution P2p spectra of PPO epoxy-amines as a function of film depth is shown in Figure 6b, where the P2p peak maxima are reported as a function of film depth. The corresponding high-resolution P2p spectra of PPO epoxy-amines before AO exposure are shown in Figure S12. It has previously been reported that the binding energy of phosphine is approximately 132 eV; furthermore, the binding energy of the phosphate structure present in the passivation layer has been determined to be approximately 134 eV.[8,30,32] Figure 6b shows that the gradient transition of phosphate formation occurred at the same depth as the [P] gradient transition observed in the XPS survey spectra results (Figure 6a). These results suggest that phosphine oxide oxidation to phosphate occurs in conjunction with the low-energy AO reactions that result in volatilization of C-based moieties. Once the reaction of phosphine oxide to phosphate achieved a steady state (e.g., 0–100 nm in sample 40–PPO), no further gradient transition was observed until atomization (Figure 6). Interestingly, sample 100–PPO exhibited a rapid transition from phosphate to virgin phosphine. Phosphine oxide is observed to be the majority component within approximately 30 nm of the surface, compared to approximately 200 nm for sample 66–PPO.

From the XPS analyses discussed above, it is apparent that the AO-irradiated PPO epoxy-amines are covered with an inert phosphate (PO_x) layer. In addition, the shift of the P2p peak from a lower binding energy of approximately 131.5 eV, corresponding to phosphine oxide (POR_3), to 133.5 eV suggests that the passivation layer is likely comprised of PO_4. These results are supported by similar observations reported in the literature.[8,30] It is expected that the PO_4 passivation layer is formed by O atom addition to P–Ph bonds. This hypothesis is also supported by the ratio of O/P shown in Figure 7. The atomic ratio of [O] to [P] was calculated from the obtained XPS survey spectra, plotted as a function of film depth, which is shown in Figure 7. First, the experimental O:P ratios of
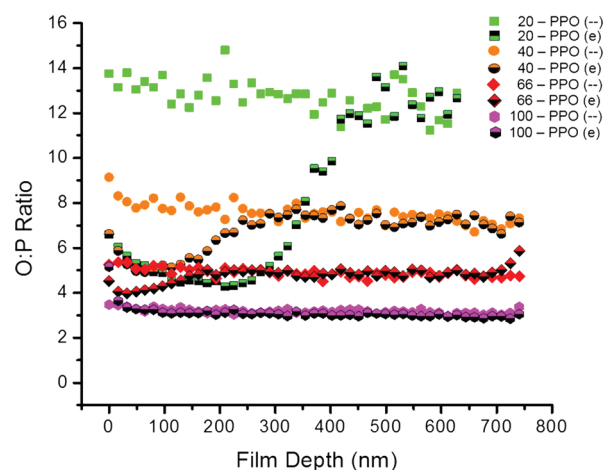

Figure 7. O:P ratios of PPO epoxy thin films measured by XPS depth profiling before (−) and after (e) exposure to an AO flux equivalent to 2.88×10^{21} O atoms·cm^{-2}.

samples unexposed to AO were in good agreement with the O:P ratios calculated from polymer empirical formulas (Table S1) and remained relatively consistent as a function of film depth. It can be observed that there is a slight decreasing trend in O:P as a function of depth across all samples, which is hypothesized to be caused by thermo-oxidative reactions occurring during polymerization. Furthermore, there is an observable amount of deviation in O:P in unexposed samples caused by small differences in atomic concentration resulting in larger deviations in O:P ratio. This deviation does not preclude valuable analyses as the return to unoxidized O:P after AO exposure remains clear and oxidized regions exhibit consistent O:P ratios. Within each analyzed sample, several noteworthy phenomena were observed: the location of the O:P minimum, the depth of low-energy AO reactions occurring deep within the polymer, and the depth of high-energy AO reactions occurring near the surface of the polymer.

The O:P minimum across all samples tends toward a value of 4:1 from the pristine polymer atomic composition, in agreement with the expected value for a PO_4 passivation layer. Furthermore, the depth of the O:P minimum is hypothesized to correspond to the region of the passivation layer wherein AO has insufficient energy to react with available moieties. The total thickness of the O:P minimum is therefore anticipated to represent the thickness of the fully formed PO_4 passivation layer. It is worth noting that the precise value of the O:P minimum varies from 4 to approximately 5 as [P] decreases, and this is expected to occur due to oxidation of aromatic functionalities that remain within the passivation layer. Figure 7 shows the formation of these minima across most samples, excluding sample 100–PPO. The thicknesses of the O:P minima appear to decrease as [P] increases: from approx. 150 nm in sample 20–PPO to a single point in sample 66–PPO. Furthermore, the appearance of the minima shifted closer to the surface of the polymer with increasing [P], indicative of full PO_4 passivation layer formation nearer to the surface of the exposed polymer. Generally, this supports the conclusion that increasing [P] decreases the overall passivation layer thickness. Interestingly, the PPO epoxy-amine with the highest [P] did not exhibit a detectable O:P minimum; instead, it is hypothesized that the fully formed passivation layer is present at the surface of the film and occurs in tandem with passivation

layer atomization, thereby not being detectable through this method.

The depth of AO reactions occurring within the polymer is observed as the transition from a low O:P back to the virgin polymer O:P. At this depth, the energy of AO is reduced and only moieties particularly prone to AO oxidation, such as alkyl moieties, are expected to participate in oxidative reactions. The thickness of this gradient transition is expected to be indicative of the formed passivation layer's efficacy at reducing the reactivity of AO with the polymer matrix. At low [P], the thickness of this layer is observed to be approximately 200 nm, with a trend of decreasing thickness to approximately 100 nm for sample 66−PPO and approximately 40 nm for sample 100−PPO. These results suggest that passivation layers formed from polymers with higher initial [P] are more effective at reducing AO diffusion into the polymer matrix and suggest that the formed passivation layers are more effective at reducing the energy of AO that diffuses into the polymer. This is further supported by the observation based on obtained AFM-IR images that passivation layers formed from polymers with higher [P] appear to be more complete, lacking cracks and crevasses at the surface, which could reduce AO diffusion into the polymer.

The depth of surface AO oxidation reactions occurring near the surface of the prepared epoxy-amine polymers is shown in Figure 7 as the gradient transition from the minimum O:P value (approximately 4−5) to a final, higher O:P value (approximately 5−7). In the prepared epoxy-amines with low initial [P], this transition is observed to occur over a depth of approximately 100 nm for sample 20−PPO. As [P] increases, the transition is observed to shorten from approximately 100 nm to 50, 20, and 10 nm for samples with 1.64, 3.51, 5.67, and 8.06 wt % P, respectively. The magnitude of the depth of this transition is hypothesized to reflect the depth wherein the formed passivation layer does not prevent the polymer from atomizing. The results of this study demonstrate that atomization cannot be fully prevented at the various [P] studied; it is expected that atomization will occur as long as the polymer of interest retains its organic components. Interestingly, the relatively constant [P] at these depths suggests that the phosphate passivation layer itself remains relatively unchanged as the epoxy-amine matrix around it undergoes significant oxidative degradation.

■ CONCLUSIONS

In this work, we have demonstrated the synthesis of novel PPO epoxide and diamine monomers. Polymerization of the prepared monomers resulted in an epoxy-amine with high (> 8 wt %) [P] and T_g (202 °C). Exposure of the prepared thin films to a cumulative AO flux of 2.88×10^{21} O atoms·cm^{-2} demonstrated the dependence of pre-AO exposure [P] on the resultant AO erosion rate of epoxy-amines. Epoxy-amines with >8 wt % P demonstrated a 100x improved erosion rate compared to epoxy-amine polymers with no P. The resultant PO_x passivation layer surface topologies and depth profiles were investigated through AFM-IR and XPS depth profiling.

It was observed through AFM-IR analysis that the surface morphology of the passivation layer formed after exposure of a PPO epoxy-amine was dependent on pre-AO exposure [P]. Epoxy-amines with low pre-AO exposure [P] (< 5 wt %) were observed to produce rough and heterogenous passivation layers with cracks and crevasses that are hypothesized to facilitate AO diffusion into the polymer matrix. Epoxy-amines

with high pre-AO exposure [P] (≥ 5 wt %) were observed to result in smoother and more homogenous passivation layers. XPS depth profiling analyses of resultant passivation layers demonstrated the effect of pre-exposure [P] on the depth and thickness of the resulting PO_4 passivation layer and oxidation reactions. It was observed that increasing pre-exposure [P] reduced the overall depth of oxidation reactions in the epoxy-amine thin film from 400 nm at low [P] to 50 nm at high [P]. Furthermore, the thickness and distance from the surface of the thin film of the PO_4 passivation layer was observed to be dependent on [P]. At low initial [P], the passivation layer was observed to be approximately 100 nm thick and formed at 250 nm from the surface of the film. At high initial [P], the PO_4 passivation layer was observed to be at the surface of the thin film and its thickness was approximately 10 nm.

Phosphine oxide-containing epoxy-amines provide an attractive and cost-effective platform for the preparation of LEO stable CFRPs. Their high T_g and excellent AO resistance render them promising candidates for applications in AO-rich environments such as LEO. The epoxy-amines prepared in this work are undergoing further evaluation through in-orbit testing in collaboration with the NASA Marshall Space Flight Center (MSFC) onboard OTV-6 to further confirm the LEO stability of these materials.

■ ASSOCIATED CONTENT

ⓢ Supporting Information

The Supporting Information is available free of charge at https://pubs.acs.org/doi/10.1021/acsapm.0c01017.

> Synthetic characterization, extended oxygen plasma etching data, thermogravimetric data, XPS spectra, AFM-IR images of control samples, and calculated and measured O:P ratios for prepared epoxy-amines (PDF).

■ AUTHOR INFORMATION

Corresponding Author

Jeffrey Wiggins − School of Polymer Science and Engineering, University of Southern Mississippi, Hattiesburg, Mississippi 39406, United States; ⓞ orcid.org/0000-0001-7662-0669; Phone: 601.266.6960; Email: jeffrey.wiggins@usm.edu

Authors

Witold K. Fuchs − School of Polymer Science and Engineering, University of Southern Mississippi, Hattiesburg, Mississippi 39406, United States

Catherine Sarantes − School of Polymer Science and Engineering, University of Southern Mississippi, Hattiesburg, Mississippi 39406, United States

Nathaniel Prine − School of Polymer Science and Engineering, University of Southern Mississippi, Hattiesburg, Mississippi 39406, United States

Xiaodan Gu − School of Polymer Science and Engineering, University of Southern Mississippi, Hattiesburg, Mississippi 39406, United States; ⓞ orcid.org/0000-0002-1123-3673

Derek L. Patton − School of Polymer Science and Engineering, University of Southern Mississippi, Hattiesburg, Mississippi 39406, United States; ⓞ orcid.org/0000-0002-8738-4750

Complete contact information is available at:
https://pubs.acs.org/10.1021/acsapm.0c01017

■ REFERENCES

(1) Gudimenko, Y.; Ng, R.; Kleiman, J.; Iskanderova, Z.; Milligan, D.; Tennyson, R. C.; Hughes, P. C. Enhancement of Space Durability of Materials and External Components through Surface Modification. *J. Spacecr. Rockets* **2004**, *41*, 326−334.

(2) Minton, T. K.; Wright, M. E.; Tomczak, S. J.; Marquez, S. A.; Shen, L.; Brunsvold, A. L.; Cooper, R.; Zhang, J.; Vij, V.; Guenthner, A. J.; Petteys, B. J. Atomic Oxygen Effects on POSS Polyimides in Low Earth Orbit. *ACS Appl. Mater. Interfaces* **2012**, *4*, 492−502.

(3) Fischer, H. R.; Tempelaars, K.; Kerpershoek, A.; Dingemans, T.; Iqbal, M.; Van Lonkhuyzen, H.; Iwanowsky, B.; Semprimoschnig, C. Development of Flexible LEO-Resistant PI Films for Space Applications Using a Self-Healing Mechanism by Surface-Directed Phase Separation of Block Copolymers. *ACS Appl. Mater. Interfaces* **2010**, *2*, 2218−2225.

(4) Verker, R.; Grossman, E.; Eliaz, N. Erosion of POSS-Polyimide Films under Hypervelocity Impact and Atomic Oxygen: The Role of Mechanical Properties at Elevated Temperatures. *Acta Mater.* **2009**, *57*, 1112−1119.

(5) Dinguirard, M., Mandeville, J.C., Van Eesbeek, M., Tighe, A.P., Durin, C., Chambers, A., Gabriel, S., Goulty, D., Roberts, G. Materials Exposure and Degradation Experiment. *Am. Inst. Aeronaut. Astronaut.* 2001, No. c.

(6) Imai, F.; Imagawa, K. Nasa's Space Environment Exposure Experiment on ISS-First Retrieval of SM/MPAC&SEED. *Eur. Sp. Agency, Special Publ ESA SP* **2003**, *2003*, 589−594.

(7) Kimoto, Y.; Ichikawa, S.; Miyazaki, E.; Matsumoto, K.; Ishizawa, J.; Shimamura, H.; Yamanaka, R.; Suzuki, M. Space Environment Effects on Materials at Different Positions and Operational Periods of ISS. *AIP Conf. Proc.* **2009**, *1087*, 207−211.

(8) Zhao, Y.; Li, G. M.; Dai, X. M.; Liu, F. F.; Dong, Z. X.; Qiu, X. P. AO-Resistant Properties of Polyimide Fibers Containing Phosphorous Groups in Main Chains. *Chinese J. Polym. Sci. English Ed.* **2016**, *34*, 1469−1478.

(9) Liu, F.; Guo, H.; Zhao, Y.; Qiu, X.; Gao, L. Enhanced Resistance to the Atomic Oxygen Exposure of POSS/Polyimide Composite Fibers with Surface Enrichment through Wet Spinning. *Eur. Polym. J.* **2018**, *105*, 115−125.

(10) Chernik, V. N.; Novikov, L. S.; Bondarenko, G. G.; Gaidar, A. I.; Smirnova, T. N. Study of Polymeric Fiber Erosion under Oxygen Plasma Beams. *Bull. Russ. Acad. Sci.: Phys.* **2010**, *74*, 268−271.

(11) Zhao, Y.; Gao, H.; Li, G. M.; Liu, F. F.; Dai, X. M.; Dong, Z. X.; Qiu, X. P. Synthesis and AO Resistant Properties of Novel Polyimide Fibers Containing Phenylphosphine Oxide Groups in Main Chain. *Chinese J. Polym. Sci. English Ed.* **2019**, *37*, 59−67.

(12) Banks, B. A.; Snyder, A.; Miller, S. K.; Demko, R. Issues and Consequences of Atomic Oxygen Undercutting of Protected Polymers in Low Earth Orbit. *Prot. Mater. Struct. from Sp. Environ.* **2004**, *5*, 235−243.

(13) Qian, M.; Xuan, X. Y. Hyperthermal Atomic Oxygen Durable Transparent Silicon-Reinforced Polyimide. *High Perform. Polym.* **2018**, *31*, 831−842.

(14) Suliga, A.; Jakubczyk, E. M.; Hamerton, I.; Viquerat, A. Analysis of Atomic Oxygen and Ultraviolet Exposure Effects on Cycloaliphatic Epoxy Resins Reinforced with Octa-Functional POSS. *Acta Astronaut.* **2018**, *142*, 103−111.

(15) Watson, K. A.; Ghose, S.; Lillehei, P. T.; Smith, J. G.; Connell, J. W. Effect of LEO Exposure on Aromatic Polymers Containing Phenylphosphine Oxide Groups. *AIP Conf. Proc.* **2009**, *1087*, 291−299.

(16) Smith, J. G.; Connell, J. W.; Hergenrother, P. M. Oxygen Plasma Resistant Phenylphosphine Oxide-Containing Poly(Arylene Ether)S. *Polymer (Guildf.)* **1994**, *35*, 2834−2839.

(17) Connell, J. W.; Jrt, J. G. S. Oxygen Plasma-Resistant Phenylphosphine Oxide-Containing Polyimides and Poly (Arylene Ether Heterocycle) S: 2. *Polymer* **1995**, *36*, 13−19.

(18) Schuler, P.; Haghighat, R.; Mojazza, H. Space Durable Polymer Threads. *High Perform. Polym.* **2016**, *11*, 113−121.

(19) Connell, J. W. The Effect of Low Earth Orbit Atomic Oxygen Exposure on Phenylphosphine Oxide-Containing Polymers. *High Perform. Polym.* **2000**, *12*, 43−52.

(20) He, Y.; Suliga, A.; Brinkmeyer, A.; Schenk, M.; Hamerton, I. Atomic Oxygen Degradation Mechanisms of Epoxy Composites for Space Applications. *Polym. Degrad. Stab.* **2019**, *166*, 108−120.

(21) Huang, M.; Li, S.; Dong, Z.; Feng, W. E. I.; Wang, X.; Gu, S. Oxygen Enrichment from Air Through Multilayer Thin Low-denstiy polyethylene films. *Appl. Poly. Sci.* **2002**, *83*, 3013−3021.

(22) Zhang, H.; Xu, M.; Li, B. Synthesis of a Novel Phosphorus-Containing Curing Agent and Its Effects on the Flame Retardancy, Thermal Degradation and Moisture Resistance of Epoxy Resins. *Polym. Adv. Technol.* **2016**, *27*, 860−871.

(23) Yasemin, A.; Doğan, M.; Bayramlı, E. The Effect of Red Phosphorus on the Fire Properties of Intumescent Pine Wood Flour−LDPE Composites Yasemin. *Fire Mater.* **2016**, *40*, 697−703.

(24) Riley, D. J. No Title, Virginia Polytechnic Institute, 1997.

(25) Zheng, N.; He, J.; Gao, J.; Huang, Y.; Besenbacher, F.; Dong, M. Adhesion Force Measured by Atomic Force Microscopy for Direct Carbon Fiber-Epoxy Interfacial Characterization. *Mater. Des.* **2018**, *145*, 218−225.

(26) Kizilkaya, C.; Karatas, S.; Apohan, N.-K.; Gungor, A. Synthesis and Characterization of Novel Polyimide/SiO2 Nanocomposite Materials Containing Phenylphosphine Oxide via Sol-Gel Technique. *J. Appl. Polym. Sci.* **2010**, *115*, 3256−3264.

(27) Mccarthy, C. E.; Banks, B. A.; De Groh, K. K.. *MISSE 2 PEACE Polymers Experiment Atomic Oxygen Erosion Yield Error Analysis.* 2010, No. November.

(28) Musto, P.; Ragosta, G.; Russo, P.; Mascia, L. Thermal-Oxidative Degradation of Epoxy and Epoxy-Bismaleimide Networks: Kinetics and Mechanism. *Macromol. Chem. Phys.* **2001**, *202*, 3445−3458.

(29) Banks, B. A.; Kneubel, C. A.; Miller, S.K.. Atomic Oxygen Energy in Low Frequency Hyperthermal Plasma Ashers. 2014, No. November.

(30) Liu, B.; Ji, M.; Liu, J.; Fan, L.; Yang, S. Phenylphosphine Oxide Containing Polyimide Matrix Resins for Atomic Oxygen-Resistant Fiber-Reinforced Composites. *High Perform. Polym.* **2013**, *25*, 907−917.

(31) Lei, X. F.; Qiao, M. T.; Tian, L. D.; Yao, P.; Ma, Y.; Zhang, H. P.; Zhang, Q. Y. Improved Space Survivability of Polyhedral Oligomeric Silsesquioxane (POSS) Polyimides Fabricated via Novel POSS-Diamine. *Corros. Sci.* **2015**, *90*, 223−238.

(32) Wei, J. H.; Gang, Z. X.; Ming, L. Q.; urRehman, S.; Wei, Z. H.; Dong, D. G.; Hai, C. C. Atomic Oxygen Resistant Phosphorus-Containing Copolyimides Derived from Bis [4-(3-Aminophenoxy)-Phenyl] Phenylphosphine Oxide. *Polym. Sci. Ser. B* **2014**, *56*, 788−798.

(33) Brunsvold, A.; Minton, T.; Gouzman, I.; Grossman, E.; Gonzalez, R. An Investigation of the Resistance of Polyhedral Oligomeric Silsesquioxane Polyimide to Atomic-Oxygen Attack. *High Perform. Polym.* **2016**, *16*, 303−318.